

# Hyperfine structure and lifetime of the $C^2\Sigma^+$ , $v = 0$ state of CH

Wim Ubachs, Gerard Meyer, J. J. ter Meulen, and A. Dymanus

*Fysisch Laboratorium, Katholieke Universiteit Nijmegen, Toernooiveld, 6525 ED Nijmegen, The Netherlands*

(Received 2 October 1985; accepted 3 December 1985)

From a laser induced fluorescence (LIF) experiment on a molecular beam of CH, we have obtained the  $b$  and  $c$  hyperfine constants, the  $\gamma$  and  $\gamma_D$  spin-rotation constants as well as accurate values for the rotational constants  $B$ ,  $D$ , and  $H$  for the  $C^2\Sigma^+$ ,  $v = 0$  state. From measurements of the linewidths, that are partially caused by predissociation, and by comparing relative line intensities, we determined different lifetimes for upper ( $F_1$ ) and lower ( $F_2$ )  $\rho$ -doublet states of the  $C^2\Sigma^+$  state. For the  $F_1$  states we find a constant lifetime of  $3.7 \pm 1.0$  ns, that is independent of  $N$ , while for the  $F_2$  states we observed an increase in lifetime for higher  $N$  up to  $8.0 \pm 1.5$  ns for  $N = 11$ .

## I. INTRODUCTION

The carbon hydride radical has been a subject of many spectroscopical as well as astrophysical investigations. From optical absorption spectra it was established a long time ago that CH is a very important constituent of stellar atmospheres. In interstellar space the first identified molecules were CH,  $CH^+$ , and  $CN^{1,2}$ ; CH was detected in the heads of comets from its fluorescence radiation induced by sunlight.<sup>3</sup> In these regions the emission and/or absorption spectra of the  $A^2\Delta-X^2\Pi$ ,  $B^2\Sigma^- - X^2\Pi$ , and  $C^2\Sigma^+ - X^2\Pi$  transitions at 430, 390, and 314 nm, respectively, are observed. Also in organic chemistry CH plays an important role; it is the emitter of the blue light in the combustion flames of all organic compounds. The CH radical is also of theoretical importance; it is a simple example of a diatomic molecule with only seven electrons in an open shell configuration, well within the capabilities of detailed *ab initio* calculations.

The optical spectra of the  $A^2\Delta-X^2\Pi$ ,  $B^2\Sigma^- - X^2\Pi$ , and  $C^2\Sigma^+ - X^2\Pi$  transitions were analyzed by Gerö.<sup>4</sup> A number of absorption spectra of CH in the vacuum ultraviolet, involving transitions to the  $D^2\Pi$ ,  $E^2\Pi$ , and  $F^2\Sigma^+$  states have been investigated in the laboratory by Herzberg and Johns.<sup>5</sup> A detailed analysis of the  $X^2\Pi$  ground state was performed by Evenson *et al.*,<sup>6</sup> who observed rotational transitions in the electronic ground state by laser magnetic resonance. The astronomers<sup>7,8</sup> succeeded first to measure the  $\Lambda$ -doublet transitions at 3.3 GHz of the lowest rotational state  $J = 1/2$  in the  $X^2\Pi$  state. Recently Bogey *et al.*<sup>9</sup> and independently Brazier and Brown<sup>10</sup> investigated the microwave spectrum of the  $X^2\Pi$  state for several rotational transitions in the laboratory and obtained accurate rotational,  $\Lambda$  doubling and hyperfine constants for the  $X^2\Pi$  state. Brazier and Brown also analyzed the hyperfine structure and  $\Lambda$  doubling in the  $A^2\Delta$  state of CH.

Predissociation of the  $C^2\Sigma^+$  state of CH was observed in several investigations.<sup>5,11-15</sup> For the low-lying electronic states of CH this process is also of astrophysical importance, as it may serve as a destruction mechanism for CH in interstellar clouds. There has been some discussion on the lifetime of the  $C^2\Sigma^+$  state, on the perturbing state responsible for the predissociation and whether  $F_1$  and  $F_2$  levels are predissociated by different rates.

In the present investigation, a molecular beam laser in-

duced fluorescence (LIF) experiment, the hyperfine structure in the  $C^2\Sigma^+$  state was resolved for the first time and accurate values for the  $\rho$ -doubling and rotational constants including centrifugal distortions were obtained. We also observed an anomalous intensity distribution in the LIF signals between transitions to upper ( $F_1$ ) and lower ( $F_2$ )  $\rho$ -doublet states in  $C^2\Sigma^+$ . The lifetimes of  $F_1$  and  $F_2$   $\rho$ -doublet states in  $C^2\Sigma^+$  were determined from an analysis of the observed linewidths. The values obtained for the relative  $F_1$  and  $F_2$  lifetimes are consistent with a strongly anomalous intensity distribution that we observed in the LIF signals from  $F_1$  and  $F_2$  states.

## II. EXPERIMENTAL

The CH molecules are produced in a glass reaction tube similar to the one used for the production of SH molecules.<sup>16</sup> From a microwave discharge (100 W at 2.45 GHz) in a mixture of  $H_2O$  and  $O_2$  atomic hydrogen and oxygen is flowing into the reaction zone where  $C_2H_2$  is added via small holes at the end of the glass tube. The production mechanism is probably the same as described by Filseth *et al.*,<sup>17</sup> who dissociated 5%  $H_2$  or 5%  $O_2$  in Ar gas mixtures in the microwave zone. They found that CH is produced in both  $A^2\Delta$  and  $X^2\Pi$  states. Intense blue chemiluminescence from the  $A^2\Delta \rightarrow X^2\Pi$  transition at 430 nm was visible from the reaction zone, indicating that at least part of the CH molecules are formed in the  $A^2\Delta$  state. Optimal production conditions were 2 mbar  $H_2O$  and 7 mbar  $O_2$  at the inlet of the glass tube, while  $C_2H_2$  at a pressure of 15 mbar was added through small holes in the glass tube, resulting in a pressure of 0.1 mbar measured near the reaction zone that was pumped by two rootpumps with a total capacity of 500  $m^3/h$ . When, instead of the  $H_2O/O_2$  mixture, only  $H_2O$  was dissociated in the discharge, the CH production decreased by a factor of 5 and the chemiluminescence disappeared. From reactions of  $C_2H_2$  with only one atomic species H or O, obtained from discharges in pure  $H_2$  or  $O_2$ , no CH signals could be observed. Attempts to produce CH in reactions with  $CH_4$  were also unsuccessful.

The glass tube was positioned in front of a 0.1 mm wide and 2 mm high boron-nitride slit opening, that forms the source of the molecular beam machine. We found it essential that the inlet holes for the acetylene gas are as close as possi-

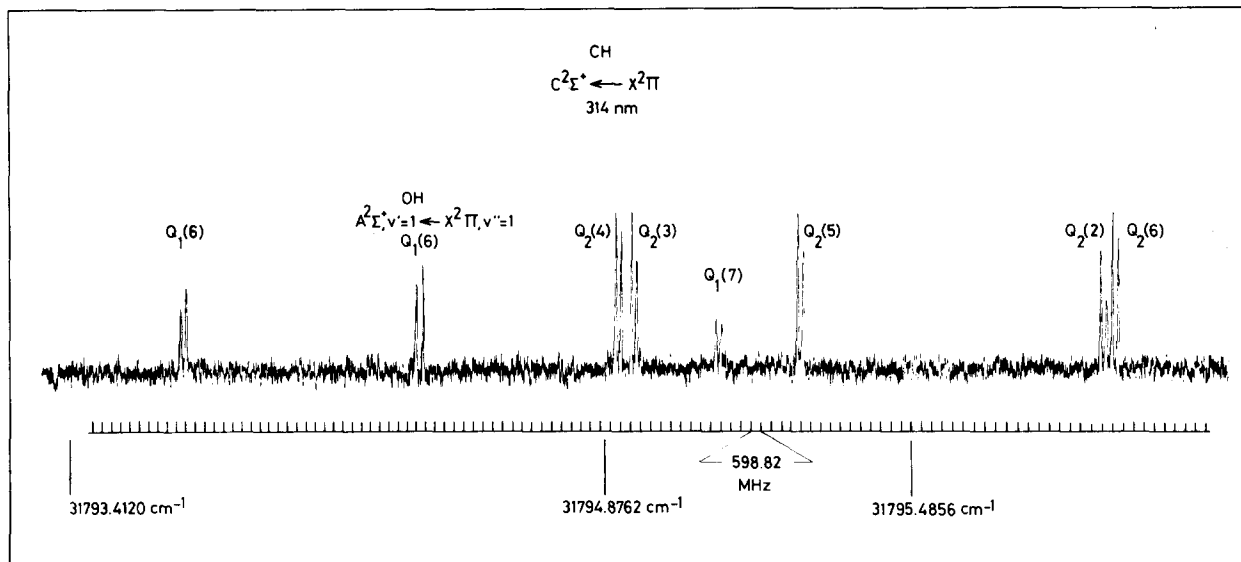


FIG. 1. Recording of part of the  $C^2\Sigma^+ \leftarrow X^2\Pi$  spectrum of CH in a 75 GHz continuous scan of the laser.

ble to the beam source, in order to avoid collisional quenching of the unstable CH radicals.

The CH molecules were excited by a perpendicularly incident UV-laser beam and detected by laser induced fluorescence (LIF) at a distance of 15 cm from the beam source in the same way as in previous investigations on SH and NH radicals.<sup>16,18</sup> The UV-laser radiation was obtained from a stabilized single frequency ring dye laser that is frequency doubled by a  $\text{LiIO}_3$  crystal inside the cavity. The measurements were performed with an average UV power of 2 mW with a bandwidth of 0.5 MHz. The molecular beam was mechanically chopped at 120 Hz in order to apply phase sensitive detection of the LIF signals. The blue chemiluminescent background radiation from the reaction zone was suppressed by UV transmission filters (Schott-UG11) in front of the photomultiplier tube. The noise was therefore determined by the stray light of the laser beam. Simultaneously with the LIF signals of the CH molecules we recorded frequency markers of a pressure and temperature stabilized interferometer for relative frequency measurements and the absorption spectrum of  $\text{I}_2$  at the fundamental laser frequency ( $\lambda = 628$  nm) for absolute frequency measurements.

### III. SPECTROSCOPY OF THE $C^2\Sigma^+$ STATE

#### A. Measurements

In total 27  $C^2\Sigma^+ \leftarrow X^2\Pi$  transitions at  $\lambda = 314$  nm

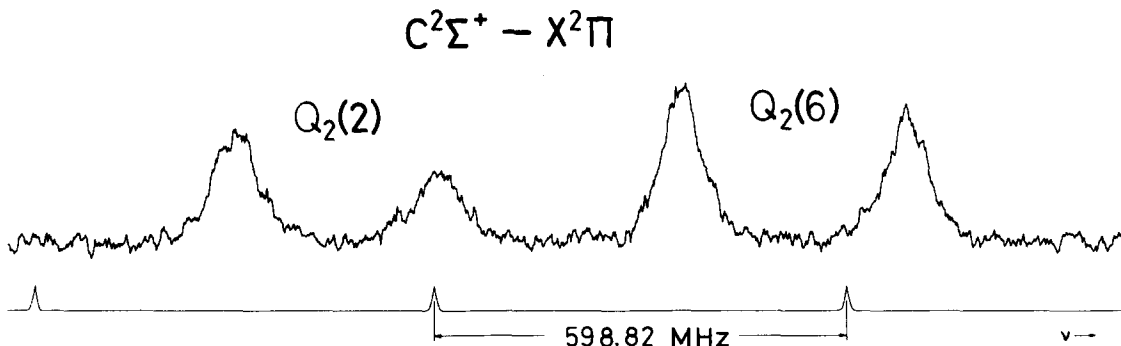


FIG. 2. Recording of the nearby lying  $C^2\Sigma^+ \leftarrow X^2\Pi$ ,  $Q_2(2)$  and  $Q_2(6)$  hyperfine doublets.

were detected. The signal-to-noise ratio was typically 20 at  $\text{RC} = 1$  s for the strongest transitions as can be seen from Fig. 1. All the spectra show a doublet structure due to the hyperfine splittings in the ground and excited state caused by the spin of the hydrogen nucleus. The hyperfine doublets for the transitions  $Q_1(N)$  for  $N = 1-7$  and 9,  $Q_2(N)$  for  $N = 2-9$ ,  $P_1(N)$  for  $N = 1, 2$ , and 4,  $P_2(N)$  for  $N = 3$  and 4,  $R_1(N)$  for  $N = 1$  and 2 and  $R_2(N)$  for  $N = 2$  and 3, and two transitions  ${}^oQ_{21}(1)$  and  ${}^oR_{11}(1)$  originating in the  $\Pi_{1/2}$ ,  $J = 1/2$  ground state were carefully recorded at least four times. Apart from these 27 also the  $Q_1(N)$  and  $Q_2(N)$  transitions up to  $N = 11$  and  $N = 19$ , respectively, could be measured, but for reasons given below these were not considered in the spectroscopic analysis. One example of a recording of the nearby lying transitions  $Q_2(2)$  and  $Q_2(6)$  is shown in Fig. 2. The hyperfine splittings that were obtained from a comparison with the simultaneously recorded markers of the external interferometer with a free spectral range (FSR) of  $299.41 \pm 0.02$  MHz at the fundamental laser frequency are listed in Table I.

Unfortunately the  $\rho$ -doublet splittings in the  $C^2\Sigma^+$  state could not be detected in single continuous laser scans because the satellite branches, such as  ${}^oP_{21}(N)$  are very weak for CH. Only the  $N = 1$   $\rho$ -doublet splitting could be obtained directly and the frequency separations between hyperfine components of upper and lower  $\rho$ -doublet states in  $N = 1$  are listed in Table II.

TABLE I. Observed hyperfine splittings (in MHz) for CH in the  $C^2\Sigma^+$ ,  $\nu=0 \leftarrow X^2\Pi$ ,  $\nu=0$  transitions.

Transition	Observed splitting
$^oQ_{21}(1)$	$224.6 \pm 9.0$
$^oR_{11}(1)$	$337.8 \pm 10.0$
$Q_1(1)$	$352.3 \pm 4.0$
$Q_1(2)$	$338.5 \pm 5.0$
$Q_1(3)$	$339.6 \pm 5.0$
$Q_1(4)$	$333.7 \pm 3.0$
$Q_1(5)$	$331.5 \pm 3.0$
$Q_1(6)$	$332.1 \pm 3.5$
$Q_1(7)$	$335.1 \pm 3.0$
$Q_1(8)$	$332.0 \pm 8.0$
$Q_1(9)$	$337.1 \pm 8.0$
$Q_2(2)$	$300.1 \pm 3.0$
$Q_2(3)$	$315.4 \pm 3.0$
$Q_2(4)$	$316.4 \pm 3.0$
$Q_2(5)$	$321.4 \pm 3.0$
$Q_2(6)$	$322.6 \pm 3.0$
$Q_2(7)$	$324.8 \pm 6.0$
$Q_2(8)$	$327.0 \pm 3.0$
$Q_2(9)$	$328.5 \pm 4.5$
$P_1(1)$	$635.0 \pm 5.0$
$P_1(2)$	$386.9 \pm 5.5$
$P_1(4)$	$362.5 \pm 3.0$
$P_2(2)$	$234.1 \pm 5.0$
$P_2(3)$	$328.8 \pm 5.0$
$P_2(4)$	$338.1 \pm 3.0$
$R_1(1)$	$350.3 \pm 3.0$
$R_1(2)$	$351.5 \pm 4.0$
$R_2(2)$	$350.5 \pm 3.0$
$R_2(3)$	$345.0 \pm 3.0$

The absolute frequencies of the transitions are obtained from frequency spacings between the CH fluorescence lines and tabulated  $I_2$  absorption lines<sup>19</sup> at the fundamental laser frequency  $\lambda = 628$  nm. The accuracy of the absolute frequencies is limited to 60–100 MHz because of the large linewidth ( $\sim 1.5$  GHz) of the iodine lines. The absolute frequencies obtained are listed in Table III. The corrections for the calibration error<sup>20</sup> of the  $I_2$  lines of  $0.0056 \text{ cm}^{-1}$  is accounted for.

In the  $Q$  branch the rotational transitions lie very close to each other, so that they can be covered in a continuous scan without mode hops of the laser. This is shown in Fig. 1 for an overview scan of 75 GHz. Especially the  $Q_2$  branch is very dense with two bandheads at  $N = 3, 4$  and  $N = 15, 16$ . These small frequency differences between rotational transitions, listed in Table IV, allow for a very accurate determination of the rotational constants in the  $C^2\Sigma^+$  state.

TABLE II. Observed splittings (in MHz) between upper and lower  $\rho$ -doublet states in the  $C^2\Sigma^+$ ,  $\nu=0$ ,  $N=1$  state of CH, and deviations from the least squares fit.

Lower state	Upper state	Observed splitting	Obs-Calc
$J=1/2, F=1$	$J=3/2, F=1$	$1684.4 \pm 8.0$	2.0
$J=1/2, F=0$	$J=3/2, F=2$	$1795.3 \pm 12.0$	-5.8

TABLE III. Observed frequencies (in  $\text{cm}^{-1}$ ) for  $C^2\Sigma^+$ ,  $\nu=0 \leftarrow X^2\Pi$ ,  $\nu=0$  transitions of CH and deviations from a least squares fit. Only the highest  $F$  hyperfine components are given.

Transition	Observed frequency	Obs-Calc
$^pQ_{11}(1)$	31 777.270 4 (60)	0.0060
$^oQ_{21}(1)$	31 805.832 9 (50)	0.0008
$^oR_{11}(1)$	31 805.9006 (80)	0.0117
$Q_1(1)$	31 788.019 8 (20)	0.0007
$Q_1(2)$	31 789.738 4 (20)	-0.0028
$Q_1(3)$	31 790.877 9 (40)	-0.0040
$Q_1(4)$	31 791.904 2 (20)	0.0009
$Q_1(5)$	31 792.930 1 (20)	0.0013
$Q_1(6)$	31 793.998 1 (20)	0.0015
$Q_1(7)$	31 795.111 7 (20)	-0.0007
$Q_1(9)$	31 797.435 9 (20)	0.0003
$P_1(1)$	31 759.475 3 (40)	0.0048
$P_1(2)$	31 732.586 7 (40)	-0.0005
$P_1(4)$	31 677.570 9 (50)	-0.0087
$R_1(1)$	31 844.990 0 (60)	0.0019
$R_1(2)$	31 874.965 0 (30)	0.0025
$Q_2(2)$	31 795.844 4 (20)	-0.0003
$Q_2(3)$	31 794.931 0 (20)	-0.0015
$Q_2(4)$	31 794.899 4 (20)	-0.0016
$Q_2(5)$	31 795.263 5 (20)	-0.0006
$Q_2(6)$	31 795.866 4 (20)	-0.0006
$Q_2(7)$	31 796.632 6 (40)	-0.0002
$Q_2(8)$	31 797.509 6 (20)	0.0002
$Q_2(9)$	31 798.452 8 (20)	0.0001
$P_2(2)$	31 738.645 5 (20)	-0.0018
$P_2(3)$	31 709.100 3 (30)	0.0043
$P_2(4)$	31 680.467 7 (30)	0.0020
$R_2(3)$	31 908.060 2 (20)	0.0006

## B. Analysis

The results of the line splittings and absolute frequencies have been fitted to an effective Hamiltonian for the  $C^2\Sigma^+$  state:

$$H = H_{\text{rot}} + H_{\text{sr}} + H_{\text{hf}}, \quad (1)$$

with

$$H_{\text{rot}} = BN^2 - DN^4 + HN^6, \quad (2)$$

TABLE IV. Frequency separations (in MHz) between rotational transitions  $C^2\Sigma^+ \leftarrow X^2\Pi$  for CH, as measured in continuous scans of the laser. The first (second) splitting is between hyperfine components lowest (highest) in frequency. In the last column the deviations from a least squares fit are given.

	Observed splitting	Obs-Calc
$Q_1(1)-Q_1(2)$	$51\,636.1 \pm 30.0$	7.8
$Q_1(4)-Q_1(5)$	$30\,754.8 \pm 10.0$	7.9
	$30\,752.6 \pm 10.0$	7.3
$Q_2(3)-Q_2(4)$	$945.6 \pm 4.0$	0.3
	$944.6 \pm 4.0$	0.3
$Q_1(7)-Q_2(5)$	$4\,885.0 \pm 8.0$	4.7
	$4\,866.8 \pm 10.0$	-4.7
$Q_2(2)-Q_2(6)$	$658.6 \pm 4.0$	-7.8
	$681.6 \pm 5.0$	11.7
$Q_1(9)-Q_2(8)$	$2\,546.9 \pm 12.0$	2.9
	$2\,536.7 \pm 10.0$	-1.1
$Q_2(8)-Q_2(9)$	$28\,280.8 \pm 10.0$	0.3
	$28\,281.4 \pm 10.0$	0.5

$$H_{sr} = (\gamma - \gamma_D N^2) \mathbf{N} \cdot \mathbf{S}, \quad (3)$$

$$H_{hf} = b \mathbf{I} \cdot \mathbf{S} + c I_z S_z, \quad (4)$$

$H_{rot}$  represents the rotational energy and centrifugal distortions in terms of the quantum number  $N$  of the molecular end over end rotation,  $H_{sr}$  gives the spin-rotation interaction

( $\rho$  doubling), also including a centrifugal distortion, and  $H_{hf}$  describes the hyperfine interaction between the electron spin and the spin  $\mathbf{I}$  of the hydrogen nucleus. On the basis of pure Hund's case (b) wave functions  $|^2\Sigma^+ NSJIF\rangle$  in the coupling scheme  $\mathbf{J} = \mathbf{N} + \mathbf{S}$ ,  $\mathbf{F} = \mathbf{J} + \mathbf{I}$  we calculated the matrix elements of the Hamiltonian  $H$  between states of equal total angular momentum  $F$ :

$$\begin{aligned} \langle ^2\Sigma^+ NJ = N - 1/2 IF = N - 1 | H | ^2\Sigma^+ N - 2 J = N - 3/2 IF = N - 1 \rangle \\ = -c\sqrt{N(N+1)}/2(2N-1), \end{aligned} \quad (5)$$

$$\begin{aligned} \langle ^2\Sigma^+ NJ = N - 1/2 IF = N - 1 | H | ^2\Sigma^+ NJ = N - 1/2 IF = N - 1 \rangle \\ = BN(N+1) - DN^2(N+1)^2 + HN^3(N+1)^3 - 1/2\gamma(N+1) \\ + 1/2\gamma_D N(N+1)^2 - 1/4\{c - b(2N-1)\}/(2N-1), \end{aligned} \quad (6)$$

$$\begin{aligned} \langle ^2\Sigma^+ NJ = N - 1/2 IF = N | H | ^2\Sigma^+ NJ = N - 1/2 IF = N \rangle \\ = BN(N+1) - DN^2(N+1)^2 + HN^3(N+1)^3 - 1/2\gamma(N+1) \\ + 1/2\gamma_D N(N+1)^2 + 1/4\{c - b(2N-1)\}/(2N+1), \end{aligned} \quad (7)$$

$$\begin{aligned} \langle ^2\Sigma^+ NJ = N - 1/2 IF = N | H | ^2\Sigma^+ NJ = N + 1/2 IF = N \rangle \\ = \langle ^2\Sigma^+ NJ = N + 1/2 IF = N | H | ^2\Sigma^+ NJ = N - 1/2 IF = N \rangle \\ = -(2b+c)\sqrt{N(N+1)}/2(2N+1), \end{aligned} \quad (8)$$

$$\begin{aligned} \langle ^2\Sigma^+ NJ = N + 1/2 IF = N | H | ^2\Sigma^+ NJ = N + 1/2 IF = N \rangle \\ = BN(N+1) - DN^2(N+1)^2 + HN^3(N+1)^3 + 1/2\gamma N \\ - 1/2\gamma_D N^2(N+1) - 1/4\{c + b(2N+3)\}/(2N+1), \end{aligned} \quad (9)$$

$$\begin{aligned} \langle ^2\Sigma^+ NJ = N + 1/2 IF = N + 1 | H | ^2\Sigma^+ NJ = N + 1/2 IF = N + 1 \rangle \\ = BN(N+1) - DN^2(N+1)^2 + HN^3(N+1)^3 + 1/2\gamma N \\ - 1/2\gamma_D N^2(N+1) + 1/4\{c + b(2N+3)\}/(2N+3). \end{aligned} \quad (10)$$

So there are contributions from matrix elements between states with  $\Delta N = \pm 2$  and  $\Delta N = 0$ ; matrix elements with  $\Delta N = 0$  and  $\Delta J = \pm 1$  represent couplings between different  $\rho$ -doublet states. There are no contributions from  $\Delta N = \pm 1$  matrix elements because the corresponding states have opposite parity and therefore do not interact.

For every rotational state  $N$  the energies of the four hyperfine states can be calculated by rearranging the matrix elements in three  $2 \times 2$  matrix blocks for  $F = N - 1$ ,  $F = N$ , and  $F = N + 1$  that can easily be diagonalized. In order to fit the observed hyperfine splittings from Table I to the calculated splittings from the matrix diagonalization the hyperfine structure in the  $^2\Pi$  states has to be regarded as well. The two lines of the observed doublet originate in different hyperfine states of  $^2\Pi$  and therefore the hyperfine splitting in the  $^2\Pi$  state has to be subtracted. Actually there are four hyperfine transitions, two of them are usually weak and overlapped by the two strong components, resulting in a hyperfine doublet. We have corrected the splittings for overlap by the weak transitions by

$$\Delta E_{cor} = \Delta E_{II,hf} I_{rel} / (1 + I_{rel}), \quad (11)$$

where  $I_{rel} = I_w/I_s$  is the calculated ratio between intensities of weak and strong transitions and  $\Delta E_{II,hf}$  is the energy distance between the two hyperfine levels in the  $X^2\Pi$  state. In all cases the overlap correction is smaller than 4 MHz, ex-

cept for the  $Q_2(2)$  transition where it is 10.5 MHz, because of the relatively large intensity of the weakest hyperfine component. By this procedure, and by averaging the results from different transitions to the same  $\rho$ -doublet state, e.g.,  $Q_2(N)$

TABLE V. Hyperfine splittings (in MHz) for CH in the  $C^2\Sigma^+$ ,  $v = 0$  state and deviations from a least squares fit.

$N$	$J$	Observed splitting	Obs-Calc
0	1/2	$617.7 \pm 5.0$	-1.8
1	1/2	$232.4 \pm 4.0$	-2.9
1	3/2	$354.0 \pm 3.0$	0.0
2	3/2	$264.0 \pm 5.0$	-1.7
2	5/2	$331.1 \pm 2.0$	-1.1
3	5/2	$278.7 \pm 3.0$	2.4
3	7/2	$323.8 \pm 2.0$	0.8
4	7/2	$280.3 \pm 3.0$	-1.7
4	9/2	$317.3 \pm 3.0$	-0.6
5	9/2	$285.6 \pm 4.0$	0.1
5	11/2	$313.0 \pm 3.0$	-1.6
6	11/2	$287.8 \pm 3.0$	-0.1
6	13/2	$312.1 \pm 4.0$	-0.3
7	13/2	$290.9 \pm 6.0$	1.2
7	15/2	$314.0 \pm 4.0$	3.3
8	15/2	$293.5 \pm 4.0$	2.5
8	17/2	$310.0 \pm 8.0$	0.6
9	17/2	$295.6 \pm 5.0$	3.5
9	19/2	$314.5 \pm 8.0$	6.2

TABLE VI. Molecular constants for CH in the  $C^2\Sigma^+$ ,  $v = 0$  state.

$\nu_{00}$	31 791.645 6 $\pm$ 0.000 5	$\text{cm}^{-1}$
$B_2$	427 382.3 $\pm$ 1.1	MHz
$D_2$	47.852 $\pm$ 0.028	MHz
$H_2$	0.002 47 $\pm$ 0.000 18	MHz
$\gamma$	1 190.7 $\pm$ 3.3	MHz
$\gamma_D$	0.667 $\pm$ 0.042	MHz
$b$	600.6 $\pm$ 1.5	MHz
$c$	56.6 $\pm$ 10.2	MHz
$b + c/3$	619.5 $\pm$ 3.5	MHz

and  $P_2(N + 1)$ , we obtained the hyperfine splittings within each  $|NJ\rangle$  state of  $C^2\Sigma^+$ . The results are listed in Table V. The data of Tables II and V were fitted to the calculated energies from the matrix diagonalization in a least squares minimalization program which yields the hyperfine constants  $b$  and  $c$ .

The rotational and hyperfine structure in the  $X^2\Pi$  ground state was calculated in the  $N$ -matrix formalism as described by Brown *et al.*<sup>21</sup> For the hyperfine parameters  $a$ ,  $b$ ,  $c$ , and  $d$ , the  $\Lambda$ -doubling parameters  $q$ ,  $q_D$ ,  $q_H$ ,  $p$ ,  $p_D$ , and  $p_H$ , the rotational constants  $B$ ,  $D$ , and  $H$  and the spin-orbit and spin-rotation constants  $A$  and  $\gamma$  we used the most recent and accurate values from a fit that incorporated all microwave and LMR data.<sup>10</sup> In a second least squares fit the data of Tables II, III, and IV were compared to the calculated values for the absolute frequencies of and the frequency separations of the  $C^2\Sigma^+ - X^2\Pi$  rotational transitions, yielding the rotational and  $\rho$ -doubling constants, including centrifugal distortions of the  $C^2\Sigma^+$  state. In spite of the precise determination of the transition frequencies and frequency separations for rotational states with  $N$  larger than 10, we did not include these data in the fit. Because of the low mass of the CH molecule, higher order centrifugal distortions for the rotation in both ground and excited state, the  $\Lambda$  doubling in the  $X^2\Pi$  state, and the  $\rho$  doubling in the  $C^2\Sigma^+$  state would be needed to obtain a reliable fit within the accuracy of the experimental data. The molecular constants for the  $C^2\Sigma^+$  state of CH obtained from the spectral data up to  $N = 9$  are listed in Table VI. In Table VII the observed absolute frequencies and in Table VIII the frequency separations of the additionally measured  $Q_2(N)$  transitions are given together with the frequencies calculated from the constants derived. The increasing differences between observed and

TABLE VII. Observed frequencies (in  $\text{cm}^{-1}$ ) for additional  $C^2\Sigma^+$ ,  $v = 0 \leftarrow X^2\Pi$ ,  $v = 0$  transitions of CH not included in the fit and deviations from calculated frequencies. Only the highest  $F$  hyperfine component is given.

Transition	Observed frequency	Obs-Calc
$Q_2(12)$	31 801.2433 (40)	- 0.0095
$Q_2(13)$	31 801.9945 (40)	- 0.0261
$Q_2(14)$	31 802.5662 (40)	- 0.0521
$Q_2(15)$	31 802.8915 (40)	- 0.0944
$Q_2(16)$	31 802.8976 (40)	- 0.1605
$Q_2(17)$	31 802.5022 (40)	- 0.2616
$Q_2(18)$	31 801.6124 (40)	- 0.4125

TABLE VIII. Observed frequency separations (in MHz) between  $C^2\Sigma^+ \leftarrow X^2\Pi$   $Q_2(N)$  transitions for CH. Only the splittings for the highest  $F$  components are given.

	Observed splitting
$Q_2(12) - Q_2(18)$	11 181.0 $\pm$ 15.0
$Q_2(18) - Q_2(13)$	11 406.6 $\pm$ 20.0
$Q_2(13) - Q_2(17)$	15 221.5 $\pm$ 15.0
$Q_2(17) - Q_2(14)$	1 922.0 $\pm$ 8.0
$Q_2(14) - Q_2(15)$	9 753.0 $\pm$ 10.0
$Q_2(15) - Q_2(16)$	183.0 $\pm$ 6.0

calculated frequencies for higher rotational states are caused by the higher order centrifugal distortions.

### C. Discussion

In the literature two possible mechanisms for the  $\rho$  doubling are discussed, a "molecular rotation effect" and a "precessing  $L$  effect." Herzberg<sup>22</sup> suggests that the rotation of the nuclei induces a magnetic field perpendicular to the internuclear axis which interacts with the electron spin  $S$ , as represented by the term  $H_{sr}$  in the effective Hamiltonian of Eq. (3). Van Vleck,<sup>23</sup> however, showed that there is a second interaction, which is dominant, except for very light molecules. In  $^2\Sigma$  states the electronic orbital momentum  $L$  can be nonzero; in the case of CH ( $^2\Sigma^+$ ) it may be considered as precessing at right angles about the axis of the molecule. By rotational distortion, a net magnetic moment results perpendicularly to the internuclear axis that also effects the electron spin. In the quantum mechanical formalism this second effect is represented by the nonzero  $\langle ^2\Sigma^+ | H | ^2\Pi \rangle$  matrix elements of the molecular Hamiltonian  $H = H_{rot} + H_{so}$  with  $H_{so} = \sum_i \zeta_i l_i \cdot s_i$  summed over the single electron spin-orbit interactions. In second order perturbation theory the following expression for the spin-rotation interaction constant is obtained:

$$\gamma = -4 \sum_{\Pi} \frac{\langle ^2\Sigma | BL_- | ^2\Pi \rangle \langle ^2\Pi | H_{so} | ^2\Sigma \rangle}{E_{\Sigma} - E_{\Pi}}, \quad (12)$$

where the summation is over all nearby lying  $^2\Pi$  states. It should be noted that  $\gamma$  is related to  $\Lambda$ -doubling constant  $p$  for the  $^2\Pi$  state:

$$p = 4 \sum_{\Sigma^s} (-)^s \frac{\langle ^2\Pi | H_{so} | ^2\Sigma^s \rangle \langle ^2\Sigma^s | BL_- | ^2\Pi \rangle}{E_{\Sigma^s} - E_{\Pi}}, \quad (13)$$

the summation is over all nearby lying  $^2\Sigma^{\pm}$  states. If only one  $\Pi$  and one  $\Sigma^s$  are interacting with each other the relation  $|p| = |\gamma|$  is obtained. It was shown by Sheasly and Matthews<sup>24</sup> that this relation holds for their experimental values for  $\text{HCl}^+$ . From Table IX it can be seen that this relation also holds quite well for OH and SH and we conclude that the "precessing  $L$  effect" gives the dominant contribution to  $\gamma$ .

In the case of CH however there are two  $\Sigma$  states,  $B^2\Sigma^-$  and  $C^2\Sigma^+$ , contributing to the  $\Lambda$  doubling in the electronic ground state which makes a comparison between  $\gamma$  and  $p$  uncertain, although the values are close to each other. A value for  $\gamma$  can be calculated from Eq. (12) in the so-called

TABLE IX. Spin-rotation constant  $\gamma$ , hyperfine constants  $b_F$ , and  $c$  in the  $^2\Sigma^+$  states and the  $A$ -doubling constant  $p$  (all in MHz) (this work and Refs. 10, 16, 25, and 26) of the OH, SH, and CH molecules, respectively.

	OH( $A^2\Sigma^+$ )	SH( $A^2\Sigma^+$ )	CH( $C^2\Sigma^+$ )
$\gamma$	6776.9	9506.7	1190.4
$p(X^2\Pi)$	7051.1	8999.6	1004.0
$b_F$	775.1	898.5	621.0
$c$	166.4	51.0	56.6

spectroscopic approximation<sup>23</sup> where the closed shell electrons in the molecules are disregarded. The molecular orbital configuration for the  $X^2\Pi$  state is  $(1s\sigma)^2(2s\sigma)^2(2p\sigma)^2(2p\pi)$ , while for the  $C^2\Sigma^+$  state we have the configuration  $(1s\sigma)^2(2s\sigma)^2(2p\sigma)(2p\pi)^2$ . The matrix elements can be evaluated by expressing the electronic wave functions in terms of Slater determinants<sup>18</sup>:

$$|X^2\Pi_{1/2}\rangle \equiv \{\sigma^+\sigma^-\pi_+\}, \quad (14)$$

$$|X^2\Pi_{-1/2}\rangle \equiv \{\sigma^+\sigma^-\pi_-\}, \quad (15)$$

$$|C^2\Sigma_{1/2}^+\rangle \equiv \frac{1}{\sqrt{2}} [\{\sigma^+\pi_-\pi_+\} - \{\sigma^+\pi_+\pi_-\}], \quad (16)$$

$$|C^2\Sigma_{-1/2}^+\rangle \equiv \frac{1}{\sqrt{2}} [\{\sigma^-\pi_-\pi_+\} - \{\sigma^-\pi_+\pi_-\}]. \quad (17)$$

The  $|^2\Pi_{3/2}\rangle$  does not give a contribution to the  $\gamma$  constant. With the wave functions (14)–(17), the result of Eq. (12) is

$$\begin{aligned} \gamma &= \frac{-2}{E_{C\Sigma^+} - E_{X\Pi}} \\ &\times [\langle ^2\Sigma_{1/2} | BL_- | ^2\Pi_{-1/2} \rangle + \langle ^2\Sigma_{-1/2} | BL_- | ^2\Pi_{1/2} \rangle] \\ &\times [\langle ^2\Pi_{1/2} | H_{so} | ^2\Sigma_{1/2} \rangle + \langle ^2\Pi_{-1/2} | H_{so} | ^2\Sigma_{-1/2} \rangle] \\ &= [\langle \pi_+ | Bl_- | \sigma^+ \rangle] / [E_{C\Sigma^+} - E_{X\Pi}] \\ &\times [\langle \sigma^- | \frac{1}{2}\zeta l_{+s} | \pi_+ \rangle + \langle \sigma^+ | \frac{1}{2}\zeta l_{-s} | \pi_+ \rangle] \\ &= \frac{2B\zeta}{E_{C\Sigma^+} - E_{X\Pi}}, \quad (18) \end{aligned}$$

where  $l_{\pm}$  and  $s_{\pm}$  represents single electron operators. With  $\zeta = 27.5 \text{ cm}^{-1}$  we obtain  $\gamma = 737 \text{ MHz}$  which is not far from the measured value. The present value for the spin-rotation constant is remarkably close to the old value of Gerö,<sup>4</sup> who found  $\gamma = 1.44 \text{ GHz}$ , while Herzberg and Johns<sup>5</sup> reported  $\gamma = 2.4 \text{ GHz}$ .

In the spectroscopic approximation both the  $b$  and  $c$  hyperfine parameters can be expressed in electron densities of only the open shell electrons.<sup>18</sup> The Fermi-contact constant  $b_F = b + c/3$  is then proportional to the electron density of the open shell electrons at the position of the hydrogen nucleus  $\langle \psi^2(\text{H}) \rangle$ :

$$b_F = 2g_H \mu_N \mu_B \langle \psi^2(\text{H}) \rangle, \quad (19)$$

where  $g_H$  is the magnetic  $g$  factor of the hydrogen nucleus,  $\mu_B$  the Bohr magneton, and  $\mu_N$  the nuclear magneton. The  $c$  constant is a measure of the sphericity of the electron charge distribution around the hydrogen nucleus:

$$c = 3g_H \mu_N \mu_B \langle (3 \cos^2 \theta - 1)/r^3 \rangle. \quad (20)$$

The CH molecule in the  $C^2\Sigma^+$  excited state has three electrons in open shells. For comparison the OH molecule in the first excited  $A^2\Sigma^+$  state has two more  $2p\pi$  electrons, resulting in a configuration with only one  $2p\sigma$  open shell electron, while SH in the  $A^2\Sigma^+$  state has eight additional electrons in closed shells and one  $3p\sigma$  open shell electron. For the open shell  $\pi$  electrons of CH the H nucleus lies in a nodal plane and so they do not contribute to the Fermi-contact term. On the other hand the unpaired  $p\sigma$  orbital has a large density on the internuclear axis and this explains the relatively large Fermi-contact constants for the three molecules of Table IX. The  $c$  constant, being inversely proportional to the cube distance of the open shell electron to the H nucleus is smaller for SH than for OH because there is an extra shell of core electrons in between the nuclei and the outer open shell electron. When comparing the  $c$  constant for CH and OH within the spectroscopic approximation one must conclude that the three open shell electron orbitals  $(2p\sigma)(2p\pi)^2$  produce a more spherical-like electron cloud than the bare  $(2p\sigma)$  orbital in OH.

To our knowledge there are no *ab initio* calculations available of the hyperfine constants for comparison with the present experimental values.

#### IV. LIFETIME OF THE $C^2\Sigma^+$ STATE

##### A. Measurements and analysis

The observed linewidths in the spectra appeared to be considerably larger than expected from residual Doppler broadening. Two OH lines, the  $A^2\Sigma^+, v=1 \leftarrow X^2\Pi, v=1, Q_1(6)$  and  $A^2\Sigma^+, v=0 \leftarrow X^2\Pi, v=0, P_1(12)$ , accidentally present in the recording showed a much narrower line profile than the CH lines. The radiative lifetime of the excited CH molecules estimated from the relative  $f$  values for the  $C^2\Sigma^+ \leftarrow X^2\Pi$  and  $A^2\Delta \leftarrow X^2\Pi$  transitions<sup>27</sup> and from the radiative lifetime for the  $A^2\Delta$  state<sup>11</sup> is 115 ns. Consequently, the observed line broadening can only be attributed to predissociation of the  $C^2\Sigma^+$  state. In order to investigate the predissociation and its dependence on the  $\rho$ -doublet and rotational states,<sup>5,11–15</sup> four series of measurements were performed:

(i) The  $A^2\Delta \leftarrow X^2\Pi$  transition was induced with a narrow band blue dye laser at  $\lambda = 430 \text{ nm}$  to probe the population of all rotational states in the  $F_1(^2\Pi_{1/2})$  and  $F_2(^2\Pi_{3/2})$  ladders. Saturation of the transition was avoided by keeping the laser power  $P_L$  below 1 mW. If the population distribution is described by a rotational temperature  $T_{\text{rot}}$  then the LIF intensities  $I_{\text{LIF}}$  of the different rotational transitions are proportional to

$$I_{\text{LIF}} \propto P_L (2J+1) S_{JJ'} e^{-E_{\text{term}}(J)/kT_{\text{rot}}}, \quad (21)$$

where  $S_{JJ'}$  is the transition moment matrix element (Hönl-London factors). In Fig. 3, the Boltzmann factors of  $F_1$  and  $F_2$  states for different  $N$  in the electronic ground state  $X^2\Pi$  are plotted. The values are calculated from observed intensities of  $A^2\Delta \leftarrow X^2\Pi Q_1(N)$  and  $Q_2(N)$  transitions by using Eq. (21). From Fig. 3, we conclude that the  $X^2\Pi$  state is thermally populated with  $T_{\text{rot}} \simeq 800 \text{ K}$  and that no anomalous distribution with regard to  $F_1$  and  $F_2$  states is present.

(ii) By reducing the opening of the rectangular slit dia-

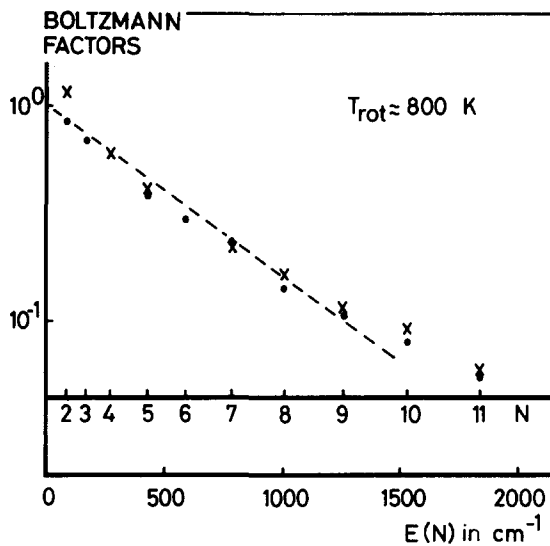


FIG. 3. Boltzmann factors for the  $X^2\Pi$ ,  $N$  states, as measured in  $A^2\Delta \leftarrow X^2\Pi$  transitions. The dots ( $\cdot$ ) refer to  $F_1$  states, the crosses ( $\times$ ) to  $F_2$  states, respectively.

phragm in the molecular beam, the linewidths of a single hyperfine component of the  $C^2\Sigma^+$ ,  $v=0 \leftarrow X^2\Pi$ ,  $v=0$ ,  $Q_1(1)$  transition and of the  $Q_1(6)$  line of OH were measured simultaneously as a function of the residual Doppler broadening. In the extrapolation to zero slit opening, we found a linewidth of  $15 \pm 3$  MHz for OH, that is mainly determined by molecular beam divergence due to the width of the source and for a minor part by the divergence of the laser beam; the

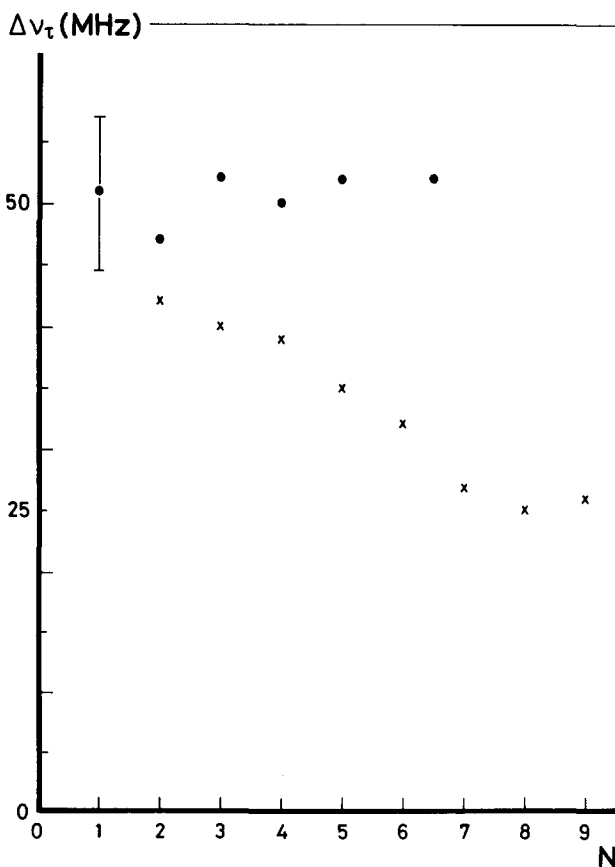


FIG. 4. Natural linewidths of  $C^2\Sigma^+$ ,  $v=0$ ,  $N$  states. The dots ( $\cdot$ ) refer to  $F_1$  states, the crosses ( $\times$ ) to  $F_2$  states, respectively.

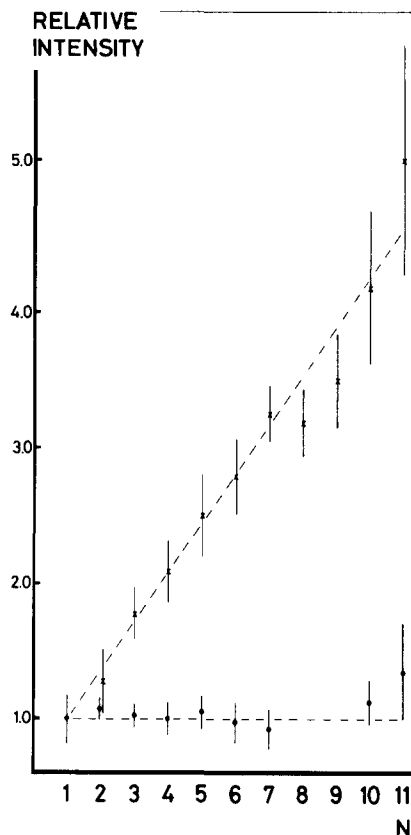


FIG. 5. Relative intensities of  $C^2\Sigma^+ \leftarrow X^2\Pi$ ,  $Q_1(N)$  and  $Q_2(N)$  transitions corrected for laser power, population of the ground state and matrix elements (Hönl-London factors). The dots ( $\cdot$ ) refer to  $F_1$  states, the crosses ( $\times$ ) to  $F_2$  states, respectively.

extrapolated linewidth was for the  $Q_1(1)$  transition in CH  $49 \pm 4$  MHz. We checked for different settings of the diaphragm that the line profile of the OH lines is indeed purely Gaussian. The broadening  $\Delta\nu_\tau$ , related to the natural lifetime of the  $C^2\Sigma^+$  state by  $\tau = 1/(2\pi\Delta\nu_\tau)$  can be evaluated from the total linewidth  $\Delta\nu_{\text{tot}}$  and Doppler contribution to the linewidth  $\Delta\nu_D$  by using the relation<sup>24</sup>:

$$\Delta\nu_\tau = \Delta\nu_{\text{tot}} - (\Delta\nu_D)^2/\Delta\nu_{\text{tot}}. \quad (22)$$

If we assume the same residual Doppler broadening  $\Delta\nu_D$  for the OH and CH radicals and average the values for  $\Delta\nu_\tau$  obtained at different diaphragm settings, we find a natural lifetime of  $\tau = 3.7 \pm 1.0$  ns for the  $C^2\Sigma^+$ ,  $N=1$ ,  $J=3/2$  state of CH.

(iii) In one geometrical configuration, with the slit diaphragm between source and LIF-zone fixed at 1.5 mm, the linewidths in the spectra of  $Q_1(N)$  and  $Q_2(N)$  lines of the  $C^2\Sigma^+ \leftarrow X^2\Pi$  transition were measured for  $N$  up to 9. From the experimental values of  $\Delta\nu_{\text{tot}}$  we subtracted via Eq. (21) an estimated Doppler contribution  $\Delta\nu_D$  of 45 MHz. This estimate is based on the measurement of the Doppler width of the OH line at this diaphragm setting. Natural linewidths for  $F_1$  and  $F_2$  levels in rotational states up to  $N=9$ , derived from these measurements are plotted in Fig. 4. The errors are determined by the uncertainty in the Doppler width and the rather large error in  $\Delta\nu_{\text{tot}}$ . Figure 4 shows clearly an  $N$ -dependent difference between the natural linewidths and therefore of the lifetime of the  $F_1$  and  $F_2$

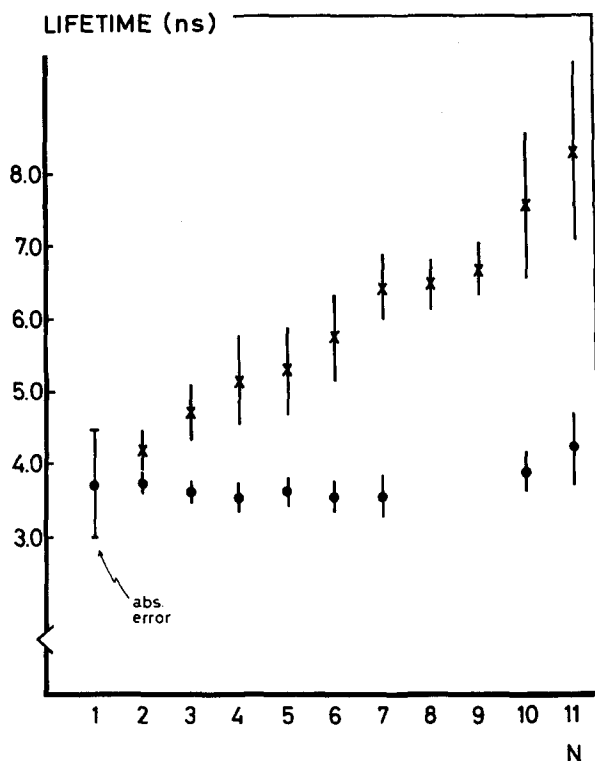


FIG. 6. Lifetimes in ns of  $C^2\Sigma^+$ ,  $N$  states as obtained from linewidth and intensity measurements. The dots ( $\cdot$ ) refer to  $F_1$  states, the crosses ( $\times$ ) to  $F_2$  states, respectively. The error bars for  $N > 1$  represent errors relative to the lifetime of the  $N = 1$ ,  $F_1$  state.

states. The natural linewidths of  $F_2$  states decreases roughly linear with  $N$ , while the  $\Delta\nu_r$  for  $F_1$  states is independent of  $N$ .

(iv) The peak intensities of  $Q_1$  and  $Q_2$  branches of the  $C^2\Sigma^+ \leftarrow X^2\Pi$  transition were measured as a function of  $N$ . The observed values were corrected for the variation of the UV-laser power and divided by calculated Hönl-London factors of the  $C^2\Sigma^+ \leftarrow X^2\Pi$  transition and by the relative population of the initial state as measured in (i). In this manner we find corrected intensities, given relatively to the  $Q_1(1)$  line that only depend on the predissociation of the excited state. Thus we find that the intensities of different  $F_1$  levels in  $C^2\Sigma^+$  do not differ, while for  $F_2$  levels we find an increase in relative intensity from 1.2 for  $N = 2$  to 5.0 for  $N = 11$ , as shown in Fig. 5.

## B. Discussion

The results for the  $N$ -dependent lifetime of the  $F_2$  states as obtained from linewidth measurements (Fig. 4) seem to disagree with the observed line intensities of the  $Q_2$  branch (Fig. 5), if line intensity is supposed to be proportional to predissociation lifetime. However, when coherent excitation to a strongly predissociated level is analyzed in terms of a simple three level scheme it follows that the relation between lifetime and peak intensity of the spectral line is a quadratic one:  $I_{\beta} \propto \tau^2$ . This relation derived in the Appendix can be explained as follows. Because of the short lifetime of the excited state, the absorption line profile is broad, while the linewidth of the laser remains much smaller ( $\Delta\nu_L < 0.5$

MHz), and as a result the absorption at the central frequency is linear with  $\tau$ . After the absorption process the competition between predissociation and fluorescence causes that only a fraction  $\tau/\tau_{\text{rad}}$  is observed. So the peak intensity of our LIF signals, that is a product of absorption and fluorescence, is proportional to  $\tau^2$ .

The  $\tau^2$  proportionality of the peak intensity explains the steeper slope in Fig. 5 than for the observed lifetimes of the  $F_2$  levels. With the quadratic behavior of the peak intensities we conclude that the values of the relative intensities agree within the error limits of the observed lifetimes. It is not possible to calculate absolute lifetimes from intensity measurements, but for the determination of relative lifetimes the intensity measurements are a very useful complementary method, because in LIF experiments intensities can be measured much more accurate than natural linewidths.

From the analysis of observed linewidths and relative line intensities we derived absolute lifetimes for  $C^2\Sigma^+$ ,  $F_1(N)$ , and  $F_2(N)$  states, that are plotted in Fig. 6.

The anomalous intensity distribution between emission from  $F_1$  and  $F_2$  states was reported by Heimer<sup>11</sup> some 50 years ago. Herzberg and Johns<sup>5</sup> were first to mention the predissociation of the  $C^2\Sigma^+$  state of CH. Under identical conditions they observed a five times weaker fluorescence yield from the  $C^2\Sigma^+ \leftarrow X^2\Pi$  transition for CH than for CD. Hesser and Lutz<sup>12</sup> produced higher resolution spectra from which they concluded that emission from  $F_1$  levels is a factor of 2-3 weaker than from  $F_2$  levels. They measured the lifetime of overlapping rotational  $F_{1,2}$  levels for  $4 < N < 12$  with the phase-shift method. As their data could not be represented by a single exponential decay two distinct lifetimes  $\tau_1 = 5$  ns and  $\tau_2 = 18$  ns were assumed, which they attributed to  $F_1$  and  $F_2$  levels, respectively. Elander and Smith<sup>13</sup> also measured phase shifts, but they probed single rotational levels in the more widely spaced  $P$  and  $R$  branches. They found a slight increase in lifetime from 6 ns for  $N = 2$  to 11 ns for  $N = 22$ , an unexplained difference in lifetime from measurements in the  $P$  and  $R$  branches, and a long lived radiative decay component of  $\tau = 80$  ns. In these measurements  $F_1$  and  $F_2$  levels were not resolved. Brzozowski *et al.*<sup>14</sup> applied the high-frequency deflection method in order to obtain the lifetime of CH ( $C^2\Sigma^+$ ). Essentially the same lifetime of 11 ns was obtained for the resolved  $F_1$  and  $F_2$  levels in the  $P_{1,2}(N)$  transitions for  $N = 2, 3$ . For  $N < 13$  they found a biexponential decay with a slow component of  $\tau = 12$  ns and a fast component of  $\tau = 3$  ns. The latter component was attributed to the  $C^2\Sigma^+, v' = 1$  state of CH. Similar biexponential decay with  $\tau_1 = 8$  ns and  $\tau_2 = 21$  ns was also observed by Ortiz and Campos<sup>15</sup> in low spectral resolution employing the delayed coincidence method. Both Ortiz and Campos<sup>15</sup> and Brzozowski *et al.*<sup>14</sup> did not detect a very slow decay with  $\tau = 80$  ns.

In the present investigation with orders of magnitude better spectral resolution we are able to give a decisive argument in the dispute on the  $N$  and  $F_{1,2}$  dependence of the lifetime of CH in the  $C^2\Sigma^+$  state. From linewidth and intensity measurements we conclude that all  $F_1$  levels up to  $N = 9$  have a lifetime  $\tau_1 = 3.7 \pm 1.0$  ns and that there is an increase in lifetime of  $F_2$  levels from  $\tau_2 = 3.8 \pm 1.0$  ns for  $N = 2$  to

$\tau_2 = 8.0 \pm 1.5$  ns for  $N = 11$ . We do not have an explanation for the relatively low absolute values for the measured lifetimes in comparison to the values reported in the literature.

Herzberg and Johns<sup>5</sup> pointed at four interacting states, three bound states  $X^2\Pi$ ,  $a^4\Sigma^-$  and  $B^2\Sigma^-$  and the repulsive  $^4\Pi$  state as the cause of the predissociation of the  $C^2\Sigma^+$  state. All these states correlate with ground state atoms  $C(^3P)$  plus  $H(^2S)$ . To our knowledge a difference in coupling between  $C^2\Sigma^+$ ,  $F_1$ , and  $F_2$  states with another potential can only be established via a spin-rotation interaction between  $B^2\Sigma^-$  and  $C^2\Sigma^+$  states. A predissociation by a  $^2\Sigma^-$  state would be a forbidden one.<sup>5,22</sup> The observed rate, being of the order of  $10^8$  s<sup>-1</sup>, is only of intermediate strength and might be caused by a forbidden predissociation.<sup>22</sup> The coupling matrix elements for a spin-rotation interaction between  $B^2\Sigma^-$  and  $C^2\Sigma^+$  states are

$$\begin{aligned} & \langle C^2\Sigma^+ NJM | H_{\gamma_{N,S}} | B^2\Sigma^- N \pm 1JM \rangle \\ &= \frac{1}{\sqrt{6}} \gamma_{00}^{1/2,1/2} - \frac{1}{\sqrt{3}} \bar{\gamma}_{00}^{1/2,1/2} \\ & \quad \times \{4 + (-)^{J+N+1/2} (J+1/2)\}, \end{aligned} \quad (23)$$

with the constants  $\gamma_{00}^{1/2,1/2}$  and  $\bar{\gamma}_{00}^{1/2,1/2}$  and the spin-rotation operator  $H_{\gamma_{N,S}}$  as defined by Freed.<sup>29</sup> According to the Fermi Golden Rule the predissociation rate of a state that interacts with another nearby lying state is proportional to the square of the absolute value of the matrix elements that couple both states:

$$\begin{aligned} 1/\tau & \propto |\langle C^2\Sigma^+ NJM | H_{\gamma_{N,S}} | B^2\Sigma^- N \pm 1JM \rangle|^2 \\ & \propto |a \pm b(N+1)|^2 \delta_{J,N \pm 1/2}, \end{aligned} \quad (24)$$

where the upper sign holds for  $F_1$  ( $J = N + 1/2$ ) levels and the lower for  $F_2$  ( $J = N - 1/2$ ); the constants  $a$  and  $b$  are derived from the  $\gamma$  constants. In the limit  $b \ll a$ , in which the  $N$  dependent term is relatively small compared to the  $N = 1$  predissociation, it follows that

$$1/\tau \propto a^2 \pm 2ab(N+1), \quad (25)$$

as was obtained also by Kovacs.<sup>30</sup> Because the sign of the constants  $\gamma_{00}^{1/2,1/2}$  and  $\bar{\gamma}_{00}^{1/2,1/2}$  and therefore of  $a$  and  $b$  can be positive or negative, Eq. (24) only shows that the lifetime of one of the two  $F_1$  and  $F_2$  components should increase linearly, while the other decreases linearly with  $N$ , if an interaction between  $^2\Sigma^+$  and  $^2\Sigma^-$  is assumed.

For the  $F_2$  levels we find an increase in lifetime linearly with  $N$ , however, for the  $F_1$  levels we find a lifetime independent of  $N$ , which is in disagreement with the prediction of Eq. (25). So the interaction with the  $B^2\Sigma^-$  state can only serve as a partial explanation for the  $F_1$  and  $F_2$  and  $N$  dependence of the predissociation in the  $C^2\Sigma^+$  state of CH. It is possible that the  $a^4\Sigma^-$ , which is not yet observed, or the repulsive  $^4\Pi$  state also causes predissociation of the  $C^2\Sigma^+$  state; the net result of two interactions might explain the  $N$  independency in the predissociation of the  $F_1$  levels.

## V. CONCLUSION

The combination of the tunable frequency doubled narrow band laser and the molecular beam technique forms a powerful instrument, not only for high resolution spectroscopy but also for the determination of lifetimes of strongly

predissociated excited states. Usually time resolved techniques cannot be used to measure lifetimes below a few nanoseconds, whereas the present method is just applicable in this domain. Furthermore it has the advantage of high resolution and collision free circumstances; one is sure not to have overlapping lines of other species. The method will not be applicable at lifetimes below a few tenths of a nanosecond because of a small fluorescence yield.

## ACKNOWLEDGMENTS

Part of this work has been supported by the Stichting voor Fundamenteel Onderzoek der Materie (FOM) and has been made possible by financial support from the Nederlandse Organisatie voor Zuiver Wetenschappelijk Onderzoek (ZWO).

## APPENDIX

We consider a molecule with a ground state  $|a\rangle$ , an excited state  $|b\rangle$ , with corresponding wave functions  $\psi_a$  and  $\psi_b$  and a predissociation channel to a third state  $|c\rangle$ , that represents the separated C and H atoms. The total wave function for the system can be written as

$$\Psi(t) = C_a(t)\psi_a + C_b(t)\psi_b + C_c(t)\psi_c, \quad (A1)$$

with  $|C_i(t)|^2$  the probability that the molecule is in state  $|i\rangle$  at time  $t$ . The rate equations for the three level system, representing transitions by coherent (de-)excitation and damping processes such as spontaneous emission and predissociation can be written as follows:

$$i\hbar\dot{C}_a(t) = 1/2C_b(t)V_{ab}, \quad (A2)$$

$$i\hbar\dot{C}_b(t) = 1/2C_a(t)V_{ba} - 1/2i\hbar\gamma C_b(t), \quad (A3)$$

$$i\hbar\dot{C}_c(t) = 1/2i\hbar\gamma C_b(t), \quad (A4)$$

where  $V_{ab} = V_{ba}^* = \langle a|\mu \cdot E|b\rangle$  is the dipole transition matrix element, and  $\gamma$  is the rate of the depopulation of the excited  $|b\rangle$  level, primarily by predissociation and for a small part by spontaneous emission. The decay rate  $\gamma$  is related to the lifetime  $\tau$ :  $\gamma = 1/\tau$ . The repopulation of the ground state  $|a\rangle$  by resonant fluorescent decay is neglected in this analysis. By differentiating Eqs. (A2) and (A3) and substituting the results two identical damped harmonic oscillator equations follow for  $C_a(t)$  and  $C_b(t)$ :

$$\ddot{C}_{a,b}(t) + 1/2\gamma\dot{C}_{a,b}(t) + 1/4\Omega^2 C_{a,b}(t) = 0, \quad (A5)$$

where  $\Omega = |V_{ab}|/\hbar$  is the characteristic Rabi frequency. With boundary conditions  $|C_a(0)|^2 = 1$  and  $|C_b(0)|^2 = 0$  we find the solution for the excited level:

$$|C_b(t)|^2 = \frac{\Omega^2 e^{-\gamma t/2}}{\gamma^2 - 4\Omega^2} \{e^{(1/4)\sqrt{\gamma^2 - 4\Omega^2}t} - e^{-(1/4)\sqrt{\gamma^2 - 4\Omega^2}t}\}^2. \quad (A6)$$

Already for moderate predissociation  $\gamma \gg \Omega$ , which is the case for the  $C^2\Sigma^+$  state of CH, and Eq. (A6) reduces to

$$|C_b(t)|^2 \simeq \Omega^2/\gamma^2 \{1 - 2e^{-\gamma t/2} + e^{-\gamma t}\}. \quad (A7)$$

In the present experiment the molecules in the molecular beam cross the interaction zone in  $10^{-6}$  s and therefore the limit  $\gamma t \gg 1$  holds. We find that the population of the excited state is proportional to the square of the lifetime:

$$|C_b(t)|^2 \simeq \Omega^2/\gamma^2 = \Omega^2\tau^2. \quad (\text{A8})$$

The fluorescence intensity  $I_{\text{fl}}$  is proportional to the population of the excited state  $|b\rangle$ :

$$I_{\text{fl}} \propto \tau^2. \quad (\text{A9})$$

<sup>1</sup>P. Swings and L. Rosenfeld, *Astrophys. J.* **86**, 483 (1937).

<sup>2</sup>W. S. Adams, *Astrophys. J.* **93**, 11 (1941).

<sup>3</sup>M. Nicolet, *Z. Astrophys.* **15**, 145 (1938).

<sup>4</sup>L. Gerö, *Z. Phys.* **118**, 27 (1941).

<sup>5</sup>G. Herzberg and J. W. C. Johns, *Astrophys. J.* **158**, 399 (1969).

<sup>6</sup>K. M. Evenson, H. E. Radford, and M. M. Moran, *Appl. Phys. Lett.* **18**, 426 (1971).

<sup>7</sup>O. E. H. Rydbeck, J. Elder, and W. M. Irvine, *Nature (London)* **246**, 466 (1973).

<sup>8</sup>B. E. Turner and B. Zuckerman, *Astrophys. J.* **187**, L59 (1974).

<sup>9</sup>M. Bogey, C. DeMuynck, and J. L. Destombes, *Chem. Phys. Lett.* **100**, 105 (1983).

<sup>10</sup>C. R. Brazier and J. M. Brown, *Can. J. Phys.* **62**, 1563 (1984).

<sup>11</sup>T. Heimer, *Z. Phys.* **78**, 771 (1932).

<sup>12</sup>J. Hesser and B. Lutz, *Astrophys. J.* **158**, 703 (1970).

<sup>13</sup>N. Elander and W. H. Smith, *Astrophys. J.* **184**, 663 (1973).

<sup>14</sup>J. Brzozowski, P. Bunker, N. Elander, and P. Erman, *Astrophys. J.* **207**, 414 (1976).

<sup>15</sup>M. Ortiz and J. Campos, *Physica C* **114**, 135 (1982).

<sup>16</sup>W. Ubachs, J. J. ter Meulen, and A. Dymanus, *Chem. Phys. Lett.* **101**, 1 (1983).

<sup>17</sup>S. V. Filseth, H. Zacharias, J. Danon, R. Wallenstein, and K. H. Welge, *Chem. Phys. Lett.* **58**, 140 (1978).

<sup>18</sup>W. Ubachs, J. J. ter Meulen, and A. Dymanus, *Can. J. Phys.* **62**, 1374 (1984).

<sup>19</sup>S. Gerstenkorn and P. Luc, *Atlas du Spectroscopie d'Absorption de la Molécule d'Iode* (CNRS, Paris, 1978).

<sup>20</sup>S. Gerstenkorn and P. Luc, *Rev. Phys. Appl.* **14**, 791 (1979).

<sup>21</sup>J. M. Brown, E. A. Colbourn, J. K. G. Watson, and F. D. Wayne, *J. Mol. Spectrosc.* **74**, 294 (1979).

<sup>22</sup>G. Herzberg, *Spectra of Diatomic Molecules* (Van Nostrand, New York, 1950).

<sup>23</sup>J. H. Van Vleck, *Phys. Rev.* **33**, 467 (1929).

<sup>24</sup>W. D. Sheasley and C. W. Matthews, *J. Mol. Spectrosc.* **47**, 420 (1973).

<sup>25</sup>J. J. ter Meulen, W. A. Majewski, W. L. Meerts, and A. Dymanus, *Chem. Phys. Lett.* **94**, 25 (1983).

<sup>26</sup>W. L. Meerts and A. Dymanus, *Can. J. Phys.* **53**, 2123 (1975).

<sup>27</sup>M. Linevsky, *J. Chem. Phys.* **47**, 3485 (1967).

<sup>28</sup>S. N. Dobryakov and Y. S. Lebedev, *Sov. Phys. Dokl.* **13**, 873 (1969).

<sup>29</sup>K. F. Freed, *J. Chem. Phys.* **45**, 4214 (1966).

<sup>30</sup>I. Kovacs, *Rotational Structure in the Spectra of Diatomic Molecules* (Hilger, London, 1969).